small NANO MICRO

Field-effect transistors

Tuning the Electrical Properties of Si Nanowire Field-Effect Transistors by Molecular Engineering

Muhammad Y. Bashouti, Raymond T. Tung, and Hossam Haick**

***E**xposed facets of n-type silicon nanowires (Si NWs) fabricated by a top-down approach are successfully terminated with different organic functionalities, including 1,3-dioxan-2-ethyl, butyl, allyl, and propyl-alcohol, using a two-step chlorination/alkylation method. X-ray photoemission spectroscopy and spectroscopic ellipsometry establish the bonding and the coverage of these molecular layers. Field-effect transistors fabricated from these Si NWs displayed characteristics that depended critically on the type of molecular termination. Without molecules the source–drain conduction is unable to be turned off by negative gate voltages as large as −20 V. Upon adsorption of organic molecules there is an observed increase in the "on" current at large positive gate voltages and also a reduction, by several orders of magnitude, of the "off" current at large negative gate voltages. The zero-gate voltage transconductance of molecule-terminated Si NW correlates with the type of organic molecule. Adsorption of butyl and 1,3-dioxan-2-ethyl molecules improves the channel conductance over that of the original SiO_2–Si NW, while adsorption of molecules with propyl-alcohol leads to a reduction. It is shown that a simple assumption based on the possible creation of surface states alongside the attachment of molecules may lead to a qualitative explanation of these electrical characteristics. The possibility and potential implications of modifying semiconductor devices by tuning the distribution of surface states via the functionality of attached molecules are discussed.*

Keywords:
- field-effect transistors
- nanowires
- silicon
- surface states
- work function

1. Introduction

Silicon nanowires (Si NWs) have emerged as a potential building material for a diverse variety of electronic devices[1,2] (e.g., p–n diodes,[2,3] bipolar junction transistors,[4] and field-effect transistors,[5] etc.), solar cells,[6,7] and chemical and biological sensors.[8,9] These small-sized Si NWs provide not only increased sensitivity, higher density devices, and better functionality but also have the potential for integration with existing Si microelectronics. Because the ability to control and predict electrical transport properties is especially important to nanoscale device applications, it is highly desirable to develop a method for fine-tuning the electrical properties of Si NWs.[10–12]

Controlled doping of Si NWs with boron (p-type) and phosphorus (n-type) has been reported.[5] Electrical transport measurements indicate reduced resistivity following doping, and that controlling the gate potential (V_g) can effectively change the conductivity of doped Si NWs. Although changes of gate potential provide temporary control of Si NW conductivity, a more permanent and robust method is desirable for Si NWs to be useful in nanoelectronic device applications.[10–12]

[*] Dr. H. Haick, Dr. M. Bashouti
The Department of Chemical Engineering and
Russell Berrie Nanotechnology Institute
Technion – Israel Institute of Technology
Haifa 32000 (Israel)
E-mail: hhossam@technion.ac.il
Prof. R. T. Tung
Department of Physics
Brooklyn College of the City University of New York
Brooklyn, NY 11210 (USA)
E-mail: rtung@brooklyn.cuny.edu

DOI: 10.1002/smll.200901402

A promising approach to control the electronic properties of Si NWs is to use polar monolayers that introduce a net electrical dipole perpendicular to the surface/interface,[13–24] modify the work function and electron affinity at a surface, and change the band offset and band bending at an interface. This functionalization effect is a general one and can be obtained with non-molecular treatments as well.[25] Nevertheless, the use of molecules, especially organic ones, allows a systematic tuning of the desired dipole moment by an appropriate choice of their functional groups[15,16,26] or the intermolecular interactions between self-assembled molecules.[24]

A surface functionalization of Si NWs with organic functionalities can be as important as the effect of the diameter and the wire orientation.[10] In fact, due to the very high surface-to-volume ratio, the functionalization of the surface and the immediate surroundings of the wire is expected to have a dominant impact on its properties. Some computational studies have shown the importance of oxygen and other passivants in Si NWs.[10–12] Similarly, the large surface-to-volume ratio in Si NWs can be exploited in Si NW functionalization and used to modify transport properties in applications such as sensors[27] and addressing arrays.[28] Si NWs tend to form a layer of SiO_2 with thickness 1–2 nm under ambient conditions, and subsequent HF treatment can be used to remove this oxide layer. Different Si surface treatments can be performed and it is also energetically favorable to passivate Si NW surfaces with organic functionalities.[29–32] However, the electrical effects of surface chemical modification of Si NW electronic structure have not been systematically investigated.

In a preliminary study, Si NWs modified by covalent $Si-CH_3$ functionality, with no intervening oxide, showed excellent atmospheric stability, high transconductance values, low surface-defect densities, and allowed for the formation of air-stable Si NW field-effect transistors (FETs) with on/off ratios in excess of 10^5 over a relatively small gate-voltage swing (± 2 V).[33] Compared to SiO_2–Si NWs, the conductance of freshly prepared H–Si NWs and of CH_3–Si NWs was much more sensitive to V_g, and could be shut-off at $V_g \approx 2.6$ V and 2.4 V, respectively, with an on/off ratio of 3.9×10^4 and 1.3×10^5. The transconductances of H–Si NWs and CH_3–Si NWs at $V_g = 0$ V were approximately four- and sevenfold higher, respectively, than that of the SiO_2–Si NWs. A cylinder-on-infinite-plate model[5] yielded estimates for μ_h of 18 ± 4 cm^2 V^{-1} s^{-1} for SiO_2–Si NW, 123 ± 3 cm^2 V^{-1} s^{-1} for H–Si NWs, and 140 ± 2 cm^2 V^{-1} s^{-1} for CH_3–Si NWs.

Here we report on an approach to fine tune the conductivity of Si NW FETs through surface modification by chlorination/alkylation functionalization procedure.[29–32,34,35] In this approach, the amorphous SiO_2 coating is first etched away by exposing Si NWs to buffered HF to form H-terminated surfaces. The H-terminated Si NWs are chlorinated, and then reacted with a variety of Grignard reagents to attach functional groups with modified characteristics, to the NW surfaces. The electrical characteristics of the molecularly modified Si NW FETs are presented and analyzed. Analyses suggest that extrinsic effects accompanying the adsorption of molecular layers, such as surface states and surface charge, may also significantly affect the FET characteristics.

2. Results

2.1. XPS, Ellipsometry, and Kelvin probe

As seen in Figure 1, the molecules used in this study have a common (C_2 alkyl) backbone and binding group (C–Si) but differ with their exposed functional groups. Figure 2 shows X-ray photoelectron spectroscopy (XPS) data from the C1s emission region of molecule-terminated 2D Si(111) samples, fitted to three peaks: C–Si at 284.11 ± 0.02 eV, C–C at 285.20 ± 0.02 eV, and C–O at 286.69 ± 0.02 eV. The peaks were typically adjusted to produce fits that minimized the difference between the full width at half-maximum (FWHM).[29–32] The center-to-center distances were fixed at 1.10 ± 0.10 eV between the C–Si and the C–C emissions and at 2.60 ± 0.10 eV between the C–O and the C–Si emissions. For a specific sample, the integrated area under the C–Si peak was constrained to maintain a fixed ratio to the integrated area under the Si2p peak (sum of $Si2p_{1/2}$ and $Si2p_{3/2}$) and normalized by scan time. The hydroxylation degree of the double bond in the allyl-Si surface was extracted from the ratio between the integrated area under the O–C–O peak (289 ± 0.02 eV) and the C–Si peak (284.11 ± 0.02).[36] The coverage of the organic functionalities were compared with the highest value obtained for methyl functionality (Figure 1a), which was found by means of scanning tunneling microscopy (STM) to represent a full coverage of the Si atop sites.[37] This comparison is expressed throughout the text as "$(C-Si/Si2p)_{molecule}/(C-Si/Si2p)_{max.methyl}$". Our XPS results showed that the $(C-Si/Si)_{molecule}/(C-Si/Si)_{max.methyl}$ ratio for all molecules was $50–60 \pm 5\%$.

Occasionally, a small signal due to oxygen was observed at 532.02 ± 0.02 eV (O1s) and assigned to adventitiously adsorbed hydrocarbons having oxygen bonded to carbon (286.69 ± 0.02 eV). It's reasonable to assume that these adventitious hydrocarbons could stem from the wet chemical processing with tetrahydrofuran (THF) solvent and THF/methanol rinse after functionalization, from carbonaceous materials present in the laboratory environment, and/or from the transportation of samples to the XPS chamber. No SiO_2 was observed in the high-resolution Si2p XPS scans, supporting the argument that the O1s signal was due to adventitious oxygen on the surface. The lack of a F1s signal in the XPS survey data, which would have appeared at 686.01 ± 0.02 eV binding energy, confirmed that the NH_4F(aq)-etched silicon surface was not terminated by Si–F species.

Excluding the methyl-terminated surfaces, ellipsometry measurements showed 0.50 ± 0.10-nm thickness of organic layers for all samples. Note that an exact determination of the absolute thickness of nanometer-thick layers by spectroscopic ellipsometry is somewhat challenging. Also, assuming isotropic optical constants for a layer composed of separate polar molecules may introduce an experimental error.

The work-function changes ($\Delta\Phi$), namely the molecule-terminated Si(111) work function as compared to the SiO_2-Si(111) work function, varied with the type of organic functionality (cf. References [15,26,38]); see Table 1. Of special interest, allyl, butyl, and 1,3-dioxan-2-ethyl functionalities exhibited negative $\Delta\Phi$ values while propyl-alcohol exhibited

NANO MICRO small

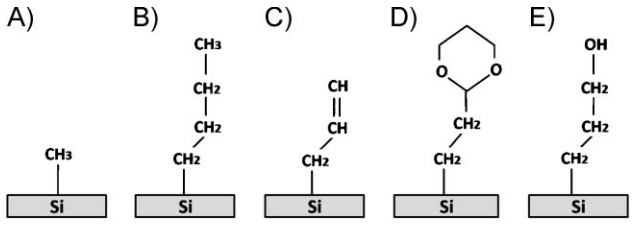

Figure 1. Schematic image of the functionalized Si surfaces. A) Methyl-Si surface; B) butyl-Si surface; C) allyl-Si surface; D) 1,3-dioxan-2-ethyl-Si surface, and E) propyl-alcohol-Si surface.

Table 1. Change in $\Delta\Phi$ due to molecule adsorption on Si(111) samples, as compared with SiO_2–Si(111). The measured work function of SiO_2–Si(111) samples was 4050 meV. The band banding was measured and found to be constant (80 ± 5 meV) in all studied samples.

Sample	$\Delta\Phi$ [meV]
Propyl-alcohol-Si(111)	$+500 \pm 50$
SiO_2–Si(111)	0 ± 50
Allyl-Si(111)	-150 ± 50
Butyl-Si(111)	-300 ± 50
1,3-dioxan-2-ethyl-Si(111)	-400 ± 50

positive $\Delta\Phi$ values. Since the coverage and binding groups to the Si surface (i.e., C–Si bond) is almost the same for all the molecules ($50–60 \pm 5\%$), the $\Delta\Phi$ could be attributed to partial electron transfer from (or to) the Si surface. These results are consistent with earlier reports that showed a decrease in the energy barrier for charge injection and thus increased device performance upon chemisorption of a polar monolayers on the surface of a semiconductor electrode.[15,16,20] A maximal $\Delta\Phi$ change ($\approx$900 meV) was obtained between propyl-alcohol-Si(111) and 1,3-dioxan-2-ethyl-Si(111) (Table 1).

2.2. Electrical Effects of Organic Functionalities

Scanning electron microscopy (SEM) images of the molecule-terminated Si NWs, integrated in a FET platform, showed similar dimensions to the SiO_2–Si NWs. However, no detectable SiO_2 was obtained by both XPS and energy-dispersive spectroscopy (EDS) on an individual fresh Si NW, consistent with our previous observations.[29–32] Figure 3 shows the current–voltage characteristics of SiO_2–Si NW FETs and butyl-Si NW FETs (as a representative example of the molecule-terminated Si NW FETs) at different gate voltages. The source–drain current (I_{sd}) of both samples increased with increasing gate voltage, indicating that the transport through the semiconducting Si NW is dominated by negative carriers (electrons), that is, the Si NW is n-type.[39]

Figure 4 shows the transconductance (g) versus back-gate voltage (V_g) in SiO_2–Si NW FET, butyl-Si NW FET, 1,3-dioxan-2-ethyl-Si NW FET, and propyl-alcohol-Si NW FET. The data presented in Figure 4 contain three distinctive features that seem to be at odds with one another and need to be explained. The first distinctive feature is an explicit dependence of the Si NW FET characteristics on the adsorbed molecules. The zero-gate voltage ($V_g = 0$), small-bias ($V_{sd} \approx 0–0.2$ V) transconductance depends on the type of absorbed molecule. Specifically, one notices the following trend: propyl-alcohol-Si NWs (0.5 ± 0.1 μS) < SiO_2–Si NWs (2.8 ± 0.4 μS) < allyl-Si NWs (7.3 ± 0.8 μS) < butyl-Si NWs (7.6 ± 0.9 μS) < 1,3-dioxan-2-ethyl-Si NWs (10.1 ± 0.6 μS), in the exact order of the $\Delta\Phi$ observed for these molecules (see Table 1). Furthermore, the threshold voltage, V_{th}, which is roughly defined as the minimum gate voltage for the low-bias conductance to reach saturation (Figure 4) correlates well with the $\Delta\Phi$, with freshly prepared 1,3-dioxan-2-ethyl, butyl, and propyl-alcohol functionalities giving rise to V_{th} values of ≈ -4 V, -2 V, and $+2$ V, respectively. These correlations seem to suggest that the influence of the molecules on the operation of the Si NW FETs is exerted through a shift in the threshold gate voltage, as if the effective work function of the gate metal, or, equivalently, the electron affinity of the Si NW, has been modified by the introduction of the molecular layer. However, such a suggestion would be difficult to rationalize because the present molecular layer does not reside between the gate and the Si NW but is located on the surface of the Si NW. While so positioned, the molecular layer is not expected to directly shift the effective gate voltage.[18] Furthermore, the sign of the observed conductance shift is opposite to

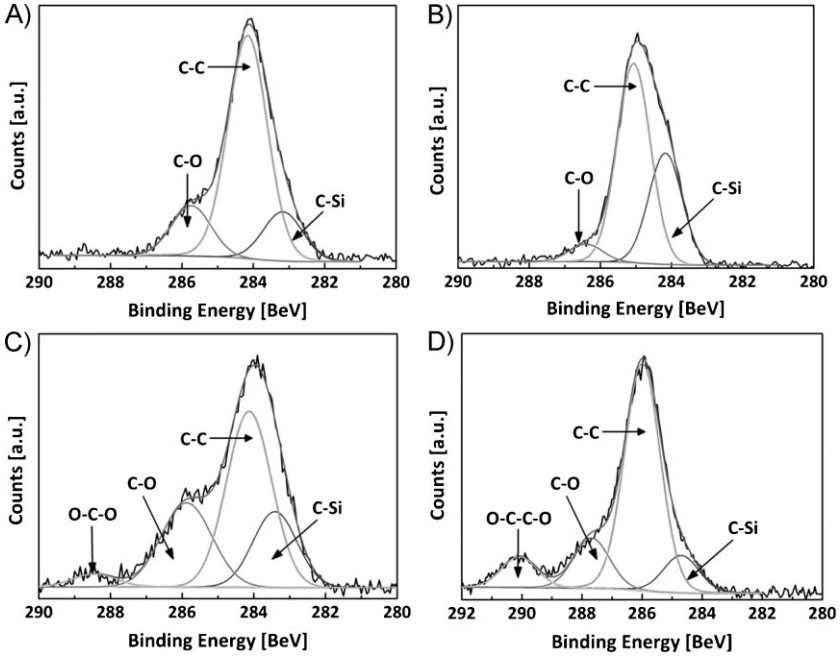

Figure 2. XPS signal of the C1s emission region from A) butyl-Si surface, B) allyl-Si surface, C) 1,3-dioxan-2-ethyl-Si surface, and D) propyl-alcohol-Si surface. Note that the XPS survey spectra of freshly prepared molecule-terminated Si samples showed Si, C, and O. For the propyl-alcohol-Si surfaces, the XPS survey showed O–C–O peaks too.[36]

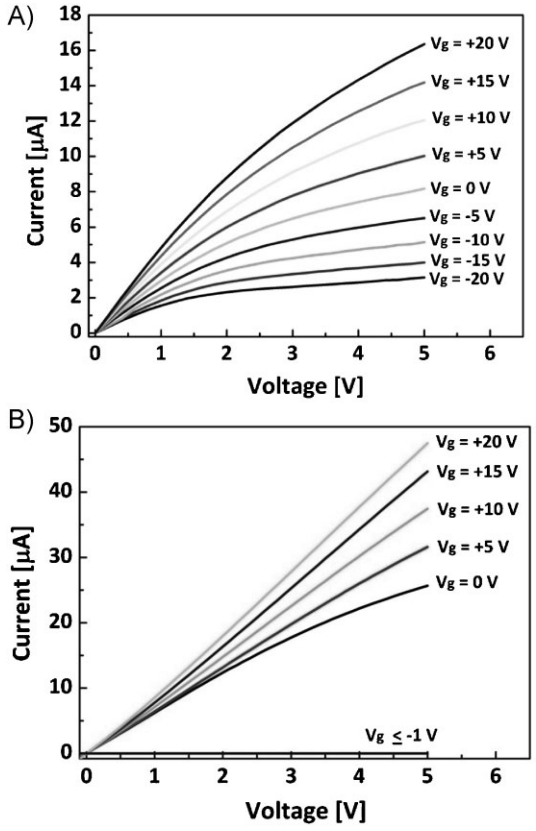

Figure 3. I–V_{ds} curves of A) SiO_2–Si NW FET and B) butyl-Si NW FET at different back-gate voltages (V_g).

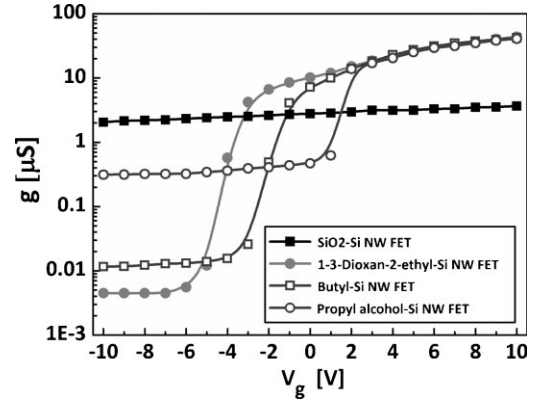

Figure 4. Transconductance (g) versus back-gate voltage (V_g) in SiO_2–Si NW FET, butyl-Si NW FET, 1,3-dioxan-2-ethyl-Si NW FET, and propyl-alcohol-Si NW FET. The tansconductance values were obatined at $V_{sd} = 0.2$ V.

the influence on the Si NW channel expected from the $\Delta\Phi$. For example, allyl, butyl, and 1,3-dioxan-2-ethyl functionalities are expected to make the conduction through the Si channel more difficult because of the reduced Si electron affinity (see Table 1)[40] but in fact an enhanced small-bias conductance was observed.

In contrast to the first distinctive feature regarding small gate-voltage characteristics, the other two distinctive features concern changes brought about by the adsorption of the molecules that are true for all molecules. The second distinctive feature is that the source–drain conductance at large, positive, gate voltages ($V_g > +3$V) is significantly enhanced from the value for SiO_2–Si NWs upon the introduction of molecules. However, this enhancement is roughly independent of either the magnitude or the sign of $\Delta\Phi$, essentially falling on the same curve in Figure 4. The third distinctive feature is that the transconductances of all molecule-terminated Si NW FET devices are significantly reduced from that of the SiO_2–Si NWs at large negative gate bias ($V_g < -5$V). For SiO_2–Si NW FETs, the transconductance decreases from 4.54 μS at $V_g = +20$ V only slightly to 1.47 μS at $V_g = -20$ V, indicating essentially an absence of on/off characteristics in this V_g region, consistent with a prior preliminary study (see Figure 4).[33] With the adsorption of molecules, the channel current is more effectively (by orders of magnitude) shut off by the negative gate voltage, resulting in a dramatic improvement in the on/off ratio of the FET device. Specifically, on/off ratios of $\approx 9 \times 10^3$, $\approx 4 \times 10^3$, and $\approx 1 \times 10^2$ are observed for 1,3-dioxan-2-ethyl-, butyl-, and propyl-alcohol-terminated Si NW FETs, respectively. One notices that models based on shifts in the threshold voltage from molecular dipolar layers are unable to explain the second and third main observations.

While the transistor characteristics for SiO_2–Si NW FETs are stable in air, properties of molecule-covered Si NW FETs were found to evolve upon air exposure. The time dependence of the average transconductance at $V_g = 0$ V of various Si NWs versus time in air are shown in Figure 5, through a normalized parameter defined as $\gamma = g_t / g_{t=0}$. For SiO_2–Si NWs, γ is constant, within experimental error, for the entire period of this investigation. For both 1,3-dioxan-2-ethyl-Si NWs and butyl-Si NWs, γ decreased with time to ≈30–40% of their initial value over a period of one month (see Figure 5). For Si NWs covered with propyl-alcohol, the observed decrease in γ was more gradual. The instability of molecule-covered Si NW FET devices also needs to be explained.

3. Discussion

3.1. Model of Surface States

We suggest that all the FET characteristics repeatedly observed experimentally and presently shown in Figures 3 and 4 may be satisfactorily explained if we consider the likelihood that, with the assembly of partial molecular layers on the Si NW channel, the density of surface states is also increased from that for SiO_2–Si NW channel. For different organic functionalities, both the density and the energy distribution of the surface states may change.[20,41,42] In the following, we make a very simple assumption on the dependence of the surface states on the type of organic functionality and show that, as a result, all the distinctive features discussed in the previous section may be qualitatively understood. For a Si surface covered by a molecular (partial) layer with a propyl-alcohol, a net negative surface charge may be found at the edges of a partial molecular layer and the ''interface'' between the molecular layer and Si NW surface (cf. Reference [20]). In the language of surface states, this is equivalent to the suggestion that the charge neutrality level (CNL)[43,44] for these surfaces may be ''lower''

NANO MICRO small

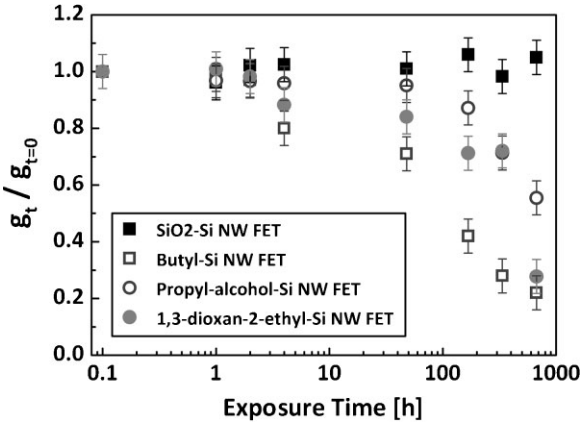

Figure 5. Normalized average conductence at $V_g = 0$ of SiO_2–Si NW FET, butyl-Si NW FET, 1,3-dioxan-2-ethyl -Si NW FET, and propyl-alcohol-Si NW FET, versus air exposure time.[69]

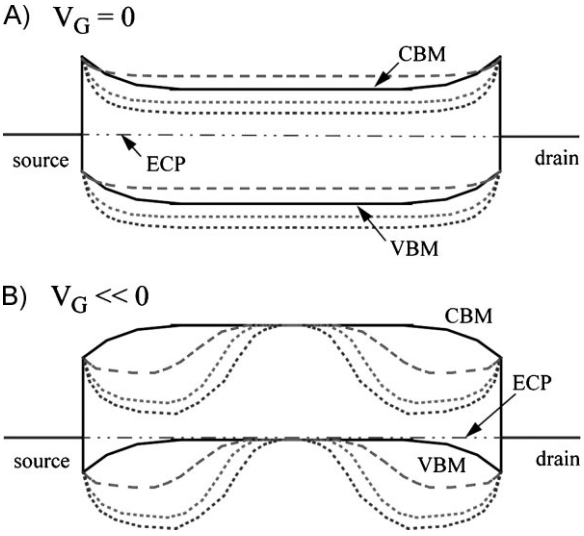

Figure 6. Expected band diagram in the near surface region of the lightly n-type doped SOI along the length of the SiO_2-passivated Si channel (solid lines), and possible band diagrams when the Si channel is covered with molecules that induce positive $\Delta\Phi$ (dashed lines) and molecules that induce negative $\Delta\Phi$ (dotted lines), plotted for a) $V_g = 0$ and b) large negative gate voltage. The electrochemical potential (ECP) is plotted as constant under small source–drain bias conditions. In (b), the bands of the unpinned, SiO_2-passivated, Si channel readily respond to the large negative gate voltage, while surface states for molecule-covered Si channels partially shield the electric field, which allows band bendings similar to the $V_g = 0$ case to be established near the metal pad regions before the valence-band maximum (VBM) is driven by the gate voltage to close to the ECP in the vicinity of the Si NW, with reduced screening.

in the Si bandgap.[45,46] Conversely, the CNL for a surface with negative molecular layer is expected to be higher in the Si bandgap. The density of surface states, which decides how tightly the local electrochemical potential/Fermi level (ECP)[47] is pinned near the CNL, should depend on the coverage of the molecular layer[12,48] (see also Reference [49]). As mentioned above, all molecules studied in the present work cover approximately 50–60 ± 5% of the Si atop sites. We therefore assume that the density of surface states (per eV, per cm^2) is approximately the same for all molecule-covered Si surfaces, with different molecules giving rise to different CNL positions.

An important consequence of a significant density of surface states for the Si NW channel is that the local ECP is pinned near the CNL of surface states. Since the SOI channel is thin (100 nm thick) and lightly doped (n-type, ≈10–20 Ω cm), the surface electrochemical potential position turns out to have a dominant effect on the conducting characteristics throughout the thickness of the channel. One may view the first, and the overriding, effect of surface states as that of dopants; in the absence of strong applied electric fields, surface states with low CNL act as p-type dopants, whereas surface states with a CNL positioned high in the Si band gap act as n-type dopants.[50] A consequence of this ''doping'' effect is illustrated in Figure 6a, where the band bending of a Si channel (with or without a NW structure) is plotted from source to drain, in the absence of either a gate voltage or a drain voltage. Si NWs covered with molecules of different organic functionalities thus behave as if the channel has different doping levels.[45] However, the surface-state mechanism differs from that of real dopants in its bi-directional nature, that is, surface states are able to drive the ECP toward the CNL from either side of the gap and much more quickly (with a x^3 dependence rather than the quadratic dependence for the space–charge region of uniformly doped semiconductor). A second important effect of surface states is the screening of electric field[51] from either side of the surface, that is, the electric field originating from either the vacuum or the silicon substrate (gate) side will be reduced across the molecular layer.[52] A third consequence of surface states is the pinning effect described above, which prevents the local ECP and, therefore, the quasi Fermi level for carriers, drifting far from the CNL. Under severe biasing conditions, the electronic transport in such a device is significantly modified from the SiO_2-passivated device because the local carrier densities are more closely tied to local specifics. In addition, the presence of surface states tends to make the metal–Si contacts ''leaky''.[53–55]

3.2. Comparison of Model with Experimental Data

To quantitatively understand the present electrical data, 3D numerical simulations are required to properly account for the electric field, band bending, surface charge, and charge transport in the Si under the metal pads, the exposed (molecule-covered) source–drain regions, the free space, and the narrow Si NW. Such simulations are under preparation as they are quite involved and not readily available. Tentatively, one notices that the surface-state model described above seems to already offer a qualitative understanding of the present electrical data. One first notes that the small gate-voltage characteristics, namely, the apparent dependence of the channel transconductance on the adsorbed molecules, is well accounted for by the apparent doping effect due to the molecules, as schematically shown in Figure 6a. The fact that the FETs are ''switched'' at different gate voltages (threshold voltages) is also expected from the apparent ''doping'' effect of the molecules. The enhanced transconductance at large positive bias can be explained by an enhanced carrier density from allyl, butyl, and 1,3-dioxan-2-ethyl functionalities and,

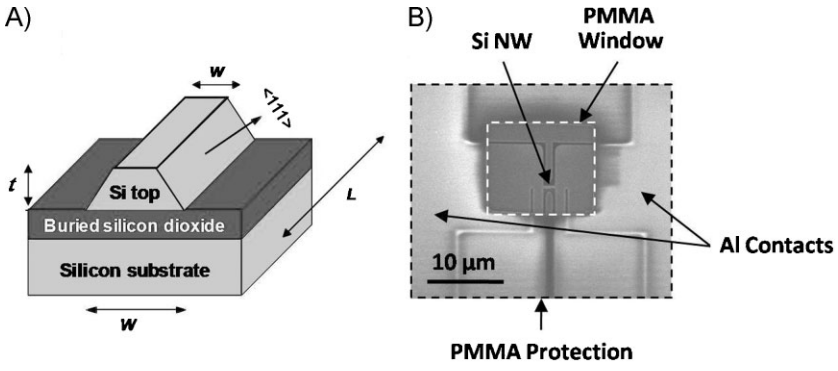

Figure 7. A) Schematics of the trapezoidal Si NW insulated from the silicon substrate by a buried SiO_2 layer. The Si NWs used in this study have a length (L) of 1 μm, a top width (w) of 70 nm, and a height (t) of 100 nm, The diagonal is based on (111) planes, whereas the small top is based on (100) plane. W (trapezoid base) = 200 nm. B) SEM image of the Si NW device, which is coated with PMMA protection layer.

probably more importantly, the much reduced contact resistance due to surface leakage.

Why the molecule-covered Si NW FETs can be turned off while the SiO_2–Si NW FET cannot is more difficult to understand. An important piece of the problem is the potential distribution around the Si NW, which is non-trivial because of the lateral pattern (Figure 7b) and the screening from surface states. Without surface pinning, the bands of the SiO_2–Si NW FET more easily respond to the gate voltage,[4] as schematically illustrated by the solid curves in Figure 6b. We speculate that surface states of molecule-covered Si channels partially shield the electric field, which allows the ECP to approach the CNL in the vicinity of the metal pad regions (cf. Figure 7b). Electric field readily penetrates the gap between source and drain, where SOI Si and surface states are absent, leading to more effective gate action near the Si NW.[56] These considerations lead to the band diagrams in Figure 6b. Note that the valence-band maximum (VBM) cannot be driven much above the ECP, as metallic screening would ensue. At large negative gate voltages, one expects that an ''effective barrier height'' is set up for conduction electrons when molecules are used, which is the difference in CBM positions between the central portion of the Si channel and the relatively flat regions near the metal pads in Figure 6b. The presence of these potential barriers is the reason for the observed on/off capability. As suggested by the schematic drawing, the effective barrier height should be larger for molecules with larger $\Delta\Phi$, in good agreement with the experiment, that is, the transconductance of 1,3-dioxan-2-ethyl-Si NW FET is observed to be smaller than that of butyl- and propyl-alcohol-terminated Si NW FETs.

Lastly, the important role played by surface states in controlling the FET characteristics, as suggested in the present model, offers a natural explanation of the electrical instability of molecule-covered Si NW devices upon air exposure (Figure 5). One assumes that the time-dependence of the FET characteristics is largely due to surface oxidation. Because electropositive entities are more prone to oxidization, one generally expects a Si surface covered with Allyl, butyl, and 1,3-dioxan-2-ethyl functionalities to oxidize more easily, because of its smaller ionization potential, than molecules with propyl-alcohol. Such a deduction would be in good agreement with the observed aging behavior of molecule-covered Si NW FETs.

3.3. Implications for Nanoscale Devices

As discussed above, a simple assumption on the correlation between the CNL of surface states distribution and the type of attached molecules has led to a qualitative explanation of all the distinctive features of the Si NW FET characteristics presently observed. While a confirmation of this dependence must await the results of more careful simulations and analyses, it seems useful to consider the implications of such a dependence, however prematurely. In recent years, there have been many proposals on the use of organic molecules to directly perform the primary tasks of, or add functionalities to, nanoelectronic devices.[15,42,57,58] In some of these investigations, the effect of the molecular layers has been attributed to the potential drop across the molecular layer and the corresponding shifts in the Schottky barrier height[59] or the band offset.[15,42,57,58] An implication of the present work, especially for incomplete molecular layers, is that surface charge and Fermi-level pinning may also be present, in addition to the potential drop across the molecular layer. A second, more constructive, implication of the present work is that incomplete molecular dipolar layers[16,19,20,60] may be used to modify the distribution of localized states on semiconductor surfaces. As the dimensions of semiconductor devices continue to decrease, interfaces and surfaces play increasingly important roles on the properties of the entire device.[10,11,61,62] An ability to tune the CNL of surface states through an adjustment of the molecular layer may be used to improve the functionality of existing devices or create new device structures. Surface states and fixed charge have traditionally been a nuisance, and yet sometimes a critical part (e.g., sensors, memories, etc.), of integrated microelectronic circuits.[63,64] Development of future quantum-effect electronics may be forced to deal with and take control of surface states. The present findings may offer a useful approach toward that effort.

4. Conclusions

Monolayers of organic molecules have been successfully attached to Si surfaces, by a two-step chlorination/alkylation method. Surface spectroscopy showed that the coverage of all the molecular layers was roughly 50–60 ± 5%. Kelvin-probe measurements showed that the Si work function was modified by the type of adsorbed molecule. FET structures, with Si NW as the main conduction path, were fabricated on thin SOI substrates and employed as the vehicle to study the effect of molecule adsorption on Si NW. FET characteristics were found to depend critically on the type of adsorbed molecule. Without molecules, that is, when the Si NW was passivated by SiO_2, the source–drain conduction was unable to be turned off by negative gate voltages as large as −20V. Upon adsorption of

NANO MICRO small

organic molecules, however, not only was there an observed increase in the ''on'' current at large positive gate voltages but there was also a reduction, by several orders of magnitude, of the ''off'' current at large negative gate voltages. The zero-gate-voltage transconductance of molecule-terminated Si NW was found to correlate with the $\Delta\Phi$ induced by the molecules. Adsorption of molecules that induce negative $\Delta\Phi$ was found to improve the channel transconductance over that of the original SiO_2–SiNW, while adsorption of molecules that induce positive $\Delta\Phi$ was found to lead to a reduction. A model was proposed, which involves the possible creation of surface states alongside the attachment of molecules, and was shown to lead to a qualitative explanation of these electrical data. In this model, a correlation of the CNL of surface states with the type of organic molecule was assumed. A major implication of the present work is the possibility of tuning electrical properties of future solid state devices by the attachment of selective molecules, if the present issue with the instability of electronic properties upon air exposure can be resolved.

5. Experimental Section

Fabrication of the FET: Si NWs were manufactured through a top-down approach. The fabrication process initiates from a bonded SOI wafer, with a thin (100 nm) top Si (100) layer (resistivity of 10–20 Ω cm) insulated from the (100) silicon substrate (resistivity of 0.8–1.2 Ω cm) by a buried silicon dioxide layer (380 nm). Mask definition was performed by high-resolution e-beam lithography. A bilayer PMMA resist was used. The exposure was performed using e-beam lithography with an acceleration voltage of 30 kV. The resist was then developed in a solution of MiBK:IPA (1:3). The pattern was transferred from the PMMA to the top SiO_2 layer by buffered HF etch. The central region, where the silicon was defined, was linked through small connections to the device leads. A 35 wt% KOH solution, saturated with isopropyl alcohol (IPA), was used. The NWs then formed in the central region. Due to the anisotropy of the silicon etch, the resulting structure had a trapezoidal cross section where the lateral sides are (111) planes. After this step, the aluminum contacts were defined by means of a lift-off process. The Si NWs, after the silicon etching, had a length (L) of 1 μm, a top width (w) of 70 nm, a height (t) of 100 nm, and W (trapezoid base) = 200 nm, as illustrated in Figure 7. The diagonal is based on (111) planes, whereas the small top is based on the (100) plane. The available starting material had a resistivity of 10–20 Ω cm (concentration about 2×10^{14}–5×10^{14} cm^{-3}). At the end of the fabrication process, the Al electrodes were coated with PMMA to protect them from etching agents (e.g., buffer HF, NH_4F, etc.) during the alkylation process.

Alkylation of the Si NW FETs and 2D Si(111): Before any chemical functionalization, each Si NW FET was cleaned by sequential N_2 gas for 10 s. After cleaning, a 10 μL drop of buffered HF (pH = 5) was placed directly on the Si NW FET for 12–20 s to etch the native oxide layer and produce a H-terminated Si NW surface. After removal of the etching drop, the sample was rinsed thoroughly with H_2O for 30 s, acetone for 1 min (to remove the polymer from the electrodes), and then H_2O for 10 s. The sample was then spin dried (5000 rpm for 30 s). A freshly etched surface was placed under a stream of chlorine gas mixture (0.4% Cl_2 and 99.6% N_2) and heated to 150 °C for 100 min to form Cl-terminated Si NW surfaces. The Si NW samples were then immersed in a (70–80 °C) solution of a Grignard reagent in THF, either in 3.0 M of methylmagnesium chloride (CH_3MgCl) to form methyl-Si NWs (Figure 2A), 2.0 M of 1-butylmagnesium chloride (CH_3-$(CH_2)_3$-MgCl) to form butyl-Si NWs (Figure 2B), 0.5 M of 1-allylmagnesium bromide ($CH=CH-CH_2$-MgBr) to form allyl-Si NWs (Figure 2C), or 0.5 M 1,3-dioxan-2-ethylmagnesium chloride ($[C_4H_8O_2]-CH_2-CH_2-MgCl$) to form 1,3-dioxan-2-ethyl-Si NWs (Figure 2D). Propyl-alcohol-Si NWs (Figure 2E) were formed by heating the sample to 50–60 °C, chlorinating the allyl-Si NW surface (Figure 2C) for 60 min, and placing the chlorinated structure in H_2O for 1 hr. 2D Si(111) surfaces, used for XPS and Kelvin probe measurements,[65] were alkylated following the procedure mentioned above but with one major difference: the samples were placed directly in HF (pH = 5) for 30 s and then in $NH_4F_{(aq)}$ 40% for 10 min to etch the native oxide layer and produce a H-terminated Si (111) surface.

XPS: The functionalized 2D Si(111) surfaces were characterized by high-resolution XPS (Thermo VG Scientific, Sigma probe, England) having a base pressure of $<3 \times 10^{-8}$ torr and fitted with a monochromatized X-ray Al Kα (1486.6 eV) source to minimize the effect of X-ray damage to the sample. The 2D Si(111) samples were first scanned from 0 to 1000 eV to monitor signals for Cl, C, and O. The Si2p at 98.0–105.0 eV, Cl2p at 198.0–204.0 eV, and C1s at 282.0–287.0 eV were investigated in detail. Scan times of up to ≈1 h were employed for data collection. The escape depth of the Si2p photoelectrons can be calculated using an empirical relation described by Seah.[66] The size of the Si atom, a_{Si}, is determined by the following equation

$$a_{si} = \left(\frac{A_{si}}{\rho_{si} N_A}\right)^{1/3} \quad (1)$$

where A_{Si} is the atomic weight of the Si (=28.086 g mol^{-1}), N_A is Avogardo's number, and ρ_{Si} is the density of Si (=2.328 g cm^{-3}). Based on these values, Equation (1) yields $a_{Si} = 0.272$ nm. The electron mean free path, λ_{Si}, was calculated from the following empirical relation

$$\lambda_{Si} = \left(\frac{0.41}{a_{Si} E_{Si}}\right) \quad (2)$$

Electron escape depth in Si has been reported to be 3.2–3.6 Å.[67] The penetration depth of the measurement can be calculated from $l_{Si} = \lambda_{Si}\sin(\alpha)$, where α is the collection angle off the surface, l_{Si} is the penetration depth, and λ_{Si} is the electron mean free path. Data presented here were collected at $\alpha = 90°$ thus yielding $l_{Si} = 3.5$ Å. For maximum measurement sensitivity, a 100 W X-ray spot of 400 μm (in diameter) with pass energies of 150 eV was used for surface survey and 20 eV was used for individual core level line scans. The photoelectron peaks of Si (100.01 ± 0.02 eV), C (284.11 ± 0.02 eV), and O (531.05 ± 0.02 eV) were measured at take-off angles (θ) of 35° and 55° between the direction of the analyzer and the specimen plane, respectively. Data analysis was performed using the Sigma Probe Advantage

software. Precise binding-energy positions and intensities were calculated by peak-fitting software (XPSPEAK version 4.1). Peak-fitting solutions were sought for $\chi^2 < 1$, where χ^2 is the standard deviation. The surface coverage of the species of interest was compared among different samples by referencing all peaks to the Si2p peak at 99.30 ± 0.01 eV. The detailed scan of the Si2p region was used to determine the number of Si oxides present/molecule coverage. The Si $2p_{1/2}$ and $Si2p_{3/2}$ peaks were fitted with two peaks held apart 0.60 ± 0.01 eV and with the $Si2p_{1/2}$:$Si2p_{3/2}$ peak area ratio maintained at 0.51.[68]

Ellipsometry measurements: The thickness of the adsorbed monolayers was measured by using a spectroscopic phase-modulated ellipsometer (M-2000V Automated Angle, J. A. Woollam Co., Inc., USA) in ambient conditions (293 K, 40% RH). Ellipsometric spectra were recorded over a range from 250–1000 nm at three different incidence angles of 65°, 70°, and 75°. The optical constants of the molecule-covered Si substrates were determined experimentally from the H-terminated Si(111) sample. A three-phase air/monolayer/substrate model was used to extract the thickness of the organic layer. We used an absorption-free Cauchy dispersion of the refractive index. The measurement was done three times for each sample and averages were taken.

Kelvin-probe measurements: Contact potential difference (CPD) of bare and molecularly modified 2D Si(111) was determined under ambient conditions (293 K) with the Ambient Kelvin Probe Package (KP Technology Ltd., UK) by measuring the electrical potential of contact-free surfaces relative to that of a (Au) reference. The Kelvin-probe package includes a head unit with integral tip amplifier, a 2-mm tip, a PCI data acquisition system, a digital electronics module, the system software, an optical baseboard with sample and Kelvin-probe mounts, a 1-inch manual translator, and a Faraday cage. The work-function resolution of the system is 1–3 mV. Data was collected for three different samples and averaged.

Electrical measurements: To assess the electrical characteristics of the various Si NW FETs, voltage-dependent back-gate measurements were performed in a probe station (Cascade Microtech Femtoguard, Summit/S300-11741B-6, USA) under ambient conditions. In these measurements, back-gate voltages (V_g) between -20 V and $+20$ V, in steps of 1 V, were applied to the silicon substrate, of which the doping level is high enough such that the band bending in the Si substrate is negligible under operating conditions. In the present device geometry (Figure 7a), over 80% of the applied gate potential is estimated to fall across the gate oxide, justifying the use of a large gate-voltage increment. For each gate voltage, the *I–V* characteristics were measured between the drain (d) and source (s) Al electrodes, contacted by a 0.5-μm radius coax probe (73Ct-CMIA/05), at a bias range of between -6 V and $+6$ V, in steps of 100 mV and/or from -0.2 to $+0.2$V in steps of 4 mV, under ambient conditions.

Acknowledgements

This research was funded by the US–Israel Binational Science Foundation (BSF), the National Science Foundation (NSF-DMR), and the Technion's Russell Berrie Nanotechnology Institute. We thank Giovanni Pennelli (Università di Pisa, Italy) and Massimo Piotto (IEIIT–Pisa, CNR, Italy) for providing initial samples. H.H. holds the Horev Chair for Leaders in Science and Technology.

[1] C. Thelander, P. Agarwal, S. Brongersma, J. Eymery, L. F. Feiner, A. Forchel, M. Scheffler, W. Riess, B. J. Ohlsson, U. Gösele, L. Samuelson, *Mater. Today* **2006**, *9*, 28.
[2] Y. Cui, C. M. Lieber, *Science* **2001**, *291*, 851.
[3] S. Hoffmann, J. Bauer, C. Ronning, T. Stelzner, J. Michler, C. Ballif, V. Sivakov, S. H. Christiansen, *Nano Lett.* **2009**, *9*, 1341.
[4] Y. Cui, Z. Zhong, D. Wang, W. U. Wang, C. M. Lieber, *Nano. Lett.* **2003**, *3*, 149.
[5] A. Morales, C. M. Lieber, *Science* **1998**, *279*, 208.
[6] V. Sivakov, G. Andrä, A. Gawlik, A. Berger, J. Plentz, F. Falk, S. H. Christiansen, *Nano Lett.* **2009**, *9*, 1549.
[7] B. Tian, X. Zheng, T. J. Kempa, Y. Fang, N. Yu, G. Yu, J. Huang, C. M. Lieber, *Nature* **2007**, *449*, 885.
[8] Y. Cui, Q. Wei, H. Park, C. M. Lieber, *Science* **2001**, *293*, 1289.
[9] J.-I. Hahm, C. M. Lieber, *Nano Lett.* **2004**, *4*, 51.
[10] P. W. Leu, B. Shan, K. Cho, *Phys. Rev. B* **2006**, *73*, 195320.
[11] C. R. Leao, A. Fazzio, A. J. R. da Silva, *Nano Lett.* **2007**, *7*, 1172.
[12] B. Aradi, L. E. Ramos, P. Deák, T. öhler, F. Bechstedt, R. Q. Zhang, T. Frauenheim, *Phys. Rev. B* **2007**, *76*, 035305.
[13] R. Cohen, N. Zenou, D. Cahen, S. Yitzchaik, *Chem. Phys. Lett.* **1997**, *279*, 270.
[14] H. Ishii, H. Sugiyama, E. Ito, K. Seki, *Adv. Mater.* **1999**, *11*, 605.
[15] G. Ashkenasy, D. Cahen, R. Cohen, A. Shanzer, A. Vilan, *Acc. Chem. Res.* **2002**, *35*, 121.
[16] H. Haick, M. Ambrico, T. Ligonzo, D. Cahen, *Adv. Mater.* **2004**, *16*, 2145.
[17] L. Frolov, Y. Rosenwaks, C. Carmeli, I. Carmeli, *Adv. Mater.* **2005**, *17*, 2434.
[18] D. Cahen, R. Naaman, Z. Vager, *Adv. Funct. Mater.* **2005**, *15*, 1571.
[19] H. Haick, M. Ambrico, T. Ligonzo, R. T. Tung, D. Cahen, *J. Am. Chem. Soc.* **2006**, *128*, 6854.
[20] A. Natan, L. Kronik, H. Haick, R. T. Tung, *Adv. Mater.* **2007**, *19*, 4103.
[21] P. Marmont, N. Battaglini, P. Lang, G. Horowitz, J. Hwang, A. Kahn, C. Amato, P. Calas, *Org. Elec.* **2008**, *9*, 419.
[22] W. Zhao, E. Salomon, Q. Zhang, S. Barlow, S. Marder, A. Kahn, *Phys. Rev. B* **2008**, *77*, 165336/1.
[23] I. Magid, L. Burstein, O. Seitz, L. Segev, L. Kronik, Y. Rosenwaks, *J. Phys. Chem. C* **2008**, *112*, 7145.
[24] Y. Paska, H. Haick, *J. Phys. Chem C* **2009**, *113*, 1993.
[25] A. Y. Anagaw, R. A. Wolkow, G. A. DiLabio, *J. Phys. Chem. C.* **2008**, *112*, 3780.
[26] R. K. Hiremath, M. K. Rabinal, B. G. Mulimani, I. M. Khazil *Langmuir* **2008**, *24*, 11300.
[27] Z. Zhong, D. Wang, Y. Cui, M. W. Bockrath, C. M. Lieber, *Science* **2003**, *302*, 1377.
[28] R. Martel, T. Schmidt, H. R. Shea, T. Hertel, P. Avouris, *Appl. Phys. Lett.* **1998**, *73*, 2447.
[29] O. Assad, S. R. Puniredd, H. Haick, *J. Am. Chem. Soc.* **2008**, *130*, 17670.
[30] M. Y. Bashouti, T. Stelzner, A. Berger, S. Christiansen, H. Haick, *J. Phys. Chem. C* **2008**, *112*, 19168.
[31] M. Y. Bashouti, T. Stelzner, A. Berger, S. Christiansen, H. Haick, *J. Phys. Chem. C* **2009**, *113*, 14823.
[32] M. Y. Bashouti, Y. Paska, S. R. Puniredd, T. Stelzner, S. Christiansen, H. Haick, *Phys. Chem. Chem. Phys.* **2009**, *11*, 3845.

[33] H. Haick, P. T. Hurley, A. I. Hochbaum, P. Yang, N. S. Lewis, *J. Am. Chem. Soc.* **2006**, *128*, 8990.
[34] S. R. Puniredd, O. Assad, H. Haick, *J. Am. Chem. Soc.* **2008**, *130*, 9184.
[35] S. R. Puniredd, O. Assad, H. Haick, *J. Am. Chem. Soc.* **2008**, *130*, 13727.
[36] A small portion of the propyl alcohol Si surfaces contain O–C–C–O segments. This could result from attacking the allyls (two) uppermost carbons (i.e, the C=C bond) with hydroxyl groups during the subsequent functionalization of the allyl Si surfaces.
[37] H. Yu, L. J. Webb, R. S. Ries, S. D. Solares, W. A. I. Goddard, J. R. Heath, N. S. Lewis, *J. Phys. Chem. B* **2005**, *109*, 671.
[38] A. Vilan, D. Cahen, *Trend. Biotechnol.* **2002**, *20*, 22.
[39] G. Zheng, W. Lu, S. Jin, C. M. Lieber, *Adv. Mater.* **2004**, *16*, 1890.
[40] O. Shaya, M. Shaked, Y. Usherenko, E. Halpern, G. Shalev, A. Doron, I. Levy, Y. Rosenwaks, *J. Phys. Chem C* **2009**, *113*, 6163.
[41] L. Kronik, Y. Shapira, *Surf. Sci. Rep.* **1999**, *37*, 1.
[42] F. Seker, K. Meeker, T. F. Kuech, A. B. Ellis, *Chem. Rev.* **2000**, *100*, 2505.
[43] H. Vazquez, F. Flores, A. Kahn, *Org. Elec.* **2007**, *8*, 241.
[44] H. Vázquez, W. Gao, F. Flores, A. Kahn, *Phys. Rev. B* **2005**, *71*, 041306/1.
[45] A. Nduwimana, X.-Q. Wang, *Nano Lett.* **2009**, *9*, 283.
[46] P. Broqvist, A. Alkauskas, A. Pasquarello, *Phys. Rev. B* **2008**, *78*, 075203/1.
[47] S. M. Sze, *Physics of Semiconductor Devices*, 2nd edition, Wiley, New York **1981**.
[48] D. Q. Fang, A. L. Rosa, T. Frauenheim, R. Q. Zhang, *Appl. Phys. Lett.* **2009**, *94*, 073116/1.
[49] D. F. Li, H. Y. Xiao, X. T. Zu, K. Z. Liu, *J. Optoelec. Adv. Mater.* **2008**, *10*, 2732.
[50] P. D. Ye, *J. Vac. Sci. Technol.* **2008**, *26*, 697.
[51] C.-T. Liang, C. G. Smith, M. Y. Simmons, D. A. Ritchie, M. Pepper, *Physica E* **2004**, *22*, 570.
[52] J. E. Inglesfield, *Philosoph. Trans. Royal Soc. London, Ser. A* **1991**, *334*, 527.
[53] A. J. Dickie, R. A. Wolkow, *Phys. Rev. B* **2008**, *77*, 115305/1.
[54] N. Kaushik, S. Haldar, M. Gupta, R. S. Gupta, *Semicond. Sci. Technol.* **2006**, *21*, 6.
[55] C. Miramond, D. Vuillaume, *J. Appl. Phys.* **2004**, *96*, 1529.
[56] D. R. Khanal, J. Wu, *Nano Lett.* **2007**, *7*, 2778.
[57] D. Cahen, G. Hodes, *Adv. Mater.* **2002**, *14*, 789.
[58] J. R. Heath, M. A. Ratner, *Phys. Today* **2003**, *56*, 43.
[59] R. T. Tung, *Mater. Sci. & Eng., R: Reports* **2001**, *R35*, 1.
[60] H. Haick, J. P. Pelz, T. Ligonzo, M. Ambrico, D. Cahen, W. Cai, C. Marginean, C. Tivarus, R. T. Tung, *Phys. Stat. Sol.* **2006**, *203*, 3438.
[61] J. Jie, W. Zhang, K. Peng, G. Yuan, C. S. Lee, S.-T. Lee, *Adv. Funct. Mater.* **2008**, *18*, 1.
[62] P.-C. Chang, C.-J. Chien, D. Stichtenoth, C. Ronning, J. G. Lua, *Appl. Phys. Lett.* **2007**, *90*, 113101/1.
[63] C. Tegenkamp, *J. Phys. Cond. Matter* **2009**, *21*, 013002/1.
[64] E. Bertel, E. Dona, *J. Phys. : Cond. Matter* **2007**, *19*, 355006/1.
[65] The diameters of the XPS beam ($\approx$400 μm) and Kelvin-probe tip ($\approx$2000 μm) are much larger than the Si NWs' top and base widths (70 nm and 200 nm, respectively). These discrepancies introduce a majority of signals that do not relate to the FETs' Si NW channel. To overcome this problem, XPS and Kelvin-probe measurements were carried out on 2D Si(111) substrates, which have much larger area than the diameters of both the XPS beam and Kelvin-probe tip. It should be noted that the exposed surface of the trapezoidal Si NW contains >70% (111) facets.
[66] M. P. Seah, *Quantification of AES and XPS*, Vol. *1*, Wiley, Chichester, UK **1990**.
[67] J. A. Haber, N. S. Lewis, *J. Phys. Chem. B* **2002**, *106*, 3639.
[68] The FWHM is a useful tool to support the identification of peak elements and to give accurate integrals of the peak area, thus increasing the accuracy of the calculation of the surface coverage.
[69] The adventitious species were observed equally for all samples. Comparing the oxidation resistance of the different samples could thus be attributed to the monolayers rather than from the additional (contamination) adlayer.

Received: August 2, 2009
Published online: September 21, 2009

